Hydrogen evolution mitigation in iron-chromium redox flow batteries via electrochemical purification of the electrolyte

Charles Tai-Chieh Wan[1,2,=], Kara E. Rodby[2,=], Mike L. Perry[3], Yet-Ming Chiang[1,4], Fikile R. Brushett[1,2,*]

[1]Joint Center for Energy Storage Research, Massachusetts Institute of Technology, Cambridge, Massachusetts 02139, United States of America
[2]Department of Chemical Engineering, Massachusetts Institute of Technology, Cambridge, Massachusetts 02139, United States of America
[3]Largo Clean Energy, Wilmington, Massachusetts 01887, United States of America
[4]Department of Materials Science and Engineering, Massachusetts Institute of Technology, Cambridge, Massachusetts 02139, United States of America

*Corresponding author: brushett@mit.edu
[=]These authors contributed equally

Abstract

The redox flow battery (RFB) is a promising electrochemical energy storage solution that has seen limited deployment due, in part, to the high capital costs of current offerings. While the search for lower-cost chemistries has led to exciting expansions in available material sets, recent advances in RFB science and engineering may revivify older chemistries with suitable property profiles. One such system is the iron-chromium (Fe-Cr) RFB, which utilizes a low-cost, high-abundance chemistry, but the poor Cr redox reaction kinetics and high hydrogen evolution reaction (HER) rates challenge efficient, long-term operation. Of late, renewed efforts have focused on HER mitigation through materials innovation including electrocatalysts and electrolyte additives. Here, we show electrochemical purification, where soluble contaminants are deposited onto a sacrificial electrode prior to cell operation, can lead to a ca. 5× reduction in capacity fade rates. Leveraging data harvested from prior literature, we identify an association between coulombic efficiency and discharge capacity decay rate, finding that electrochemical purification can enable cell performance equivalent to that with new and potentially-expensive materials. We anticipate this method of mitigating HER may reduce capacity maintenance needs and, in combination with other advances, further durational Fe-Cr RFBs.

Keywords: iron-chromium redox flow battery; electrochemical energy storage; electrochemical purification; hydrogen evolution; capacity fade

Introduction

Of the range of energy storage solutions needed to decarbonize and fortify the electric power sector, redox flow batteries (RFBs), a promising electrochemical technology, hold promise for longer duration (i.e., > 4 hours) applications. This is because the system architecture enables independent specification of energy and power ratings by storing fluidic electrolytes in external tanks and pumping them through the electrochemical stack where the soluble charge-storage species are oxidized and reduced to charge and discharge the battery. As a technology platform, RFBs can support a wide range of reduction-oxidation ("redox") couples or chemistries, but the majority of research, development, and deployment efforts have focused on the vanadium RFB (VRFB). A uniquely enabling feature of the VRFB is its symmetric chemistry, specifically the use of four water-soluble oxidation states derived from a single parent compound for the negative (V^{2+}/V^{3+}) and positive ($VO^{2+}(V^{4+})/VO_2^{+}(V^{5+})$) electrolytes. This, in turn, facilitates lifelong, low-cost capacity fade remediation [1,2]. Crossover, the undesirable transport of active species through the semi-permeable membrane that separates the positive and negative electrolytes within the stack, is the dominant form of capacity fade in most advanced RFB systems [3]. For a battery with a symmetric chemistry, such crossover can be managed via rebalancing (remixing and recharging the electrolytes), an inexpensive, simple, and automatable process [2,4]. Despite benefitting from low cost maintenance, RFB deployment remains a modest fraction of both announced and operational global energy storage systems [1], primarily due to the high upfront costs and perceived risks of current commercial options led by VRFB systems [5,6]. In particular, the high and volatile price of vanadium remains a significant obstacle to adoption [7], as the cost of the electrolyte alone (ca. 125 \$ $(kWh)^{-1}$, with fluctuations from 25 – 450 \$ $(kWh)^{-1}$ since 1980) [2] is close to the United States Department of Energy targets for the total installed system costs (generally cited between 100 and 150 \$ $(kWh)^{-1}$, and inclusive of the electrolyte, electrochemical stack, balance-of-plant components, and grid connections) [8,9]. This has catalyzed research into new RFB chemistries that utilize low-cost and high-abundance active materials including commodity-scale inorganic materials (e.g., iron, sulfur) and engineered compounds enabled by molecular functionalization (e.g., redox-active organic molecules, metal-centered coordination complexes). As a relatively new storage concept, most efforts have thus far focused on proof-of-principle demonstrations and refinement of electrochemical and physicochemical properties at the component-level. While promising, these emerging materials face an array of challenges. First, most chemistries are not inherently symmetric, employing different redox couples on either side of the electrochemical cell, which means cross-contamination due to active species crossover can be technically and/or financially difficult to prevent or remediate [3]. Second, organic molecules and coordination complexes exhibit finite decay rates under typical operating conditions that cause further capacity loss, which is similarly difficult to address [10]. Third, many proposed chemistries exhibit other unfavorable technical attributes, such as relatively low

open-circuit voltages (OCVs), variable solubility in different oxidation states, and limited ionic conductivity, that result in reduced energy/power densities and poor efficiencies [11].

Though not a new chemistry, the iron-chromium (Fe-Cr) RFB system appears promising as it seemingly avoids or mitigates many of these aforementioned challenges. Specifically, it utilizes active materials that are abundant, low cost, and stable under RFB operating conditions, and can remediate crossover losses by utilizing a mixed electrolyte configuration (also known as the "spectator strategy") [3]. Iron is the most abundant element in the Earth (by mass), and there is almost 1,000× more terrestrial chromium than vanadium [12]. Since late 2019, the price of ferrochromium – produced in a range of locations throughout Asia, Africa, Europe and the Middle East – has remained under one dollar per pound of chromium content [13]. Additionally, this mineral precursor contains forms of both active species (i.e., Fe and Cr), a potentially cost-saving feature, which could minimize waste and reduce the number of separations and other process steps needed to convert the precursor to electrochemical grade electrolyte (since it is ultimately employed as a mixed electrolyte) [14,15]. As elemental species, neither Fe nor Cr decompose, and crossover is remediable via the spectator strategy electrolyte configuration where the two electrolyte tanks contain both active species in equal concentrations, making it "pseudo-symmetric." This general operating approach is only employable if both active species are stable in the (electro)chemical environment of the opposing half-cell but, if such conditions are met and in the absence of other forms of electrolyte degradation, it enables utilization of the same or substantially similar methods pioneered for crossover remediation in VRFBs. The spectator strategy also lowers crossover rates: by having all active species ($Fe^{2+/3+}$ and $Cr^{3+/2+}$) present in nearly-equal concentrations on either side of the membrane, the diffusional driving force for crossover is diminished, which, in turn, significantly reduces the net crossover rate [14]. This approach is particularly important for the Fe-Cr system, as the Fe^{n+} and Cr^{n+} cations are ~20× more permeable than vanadium cations in Nafion™ membranes, the current state-of-the-art for RFBs [16]. Further, the ability to utilize rebalancing can enable economically viable replacement of these more expensive membranes (e.g., Nafion™) with lower-cost but less-selective options (e.g., size-exclusion membranes, non-fluorinated membranes) [2,6]. Although the chemical configuration of the spectator strategy essentially doubles the amount of active materials required and sacrifices energy density (as the solubility of true active materials is reduced due to presence of spectators) and thus increases the electrolyte cost, with sufficiently inexpensive charge-storage compounds this tradeoff may not be prohibitive. For the Fe-Cr system, utilizing the calculations by Rodby *et al*. (and adjusting the depth-of-discharge to reflect the data in the peer-reviewed Fe-Cr RFB literature – 60%, shown in **Table 1** (*vide infra*) – as opposed to the 80% used in the original work), the total electrolyte cost is only ~ 31 \$ $(kWh)^{-1}$ [10]. Thus, this RFB chemistry may represent a viable alternative to the VRFB, at least from an electrolyte cost perspective [6,10]. Further, from a practical standpoint, this system has been successfully demonstrated with the

spectator strategy in the past [14], although several technical hurdles remain that challenge the economic viability of long-term operation.

Generally considered to be the first modern RFB, the Fe-Cr system was initially advanced by the National Aeronautics and Space Administration (NASA) in the 1970s and 1980s as a potential energy storage solution for deep-space missions [17]. The system uses the following positive and negative electrode half reactions with all cationic species soluble in the aqueous phase:

Positive electrode: $$Fe^{3+} + e^- \underset{\text{charge}}{\overset{\text{discharge}}{\rightleftharpoons}} Fe^{2+} \qquad E^0 = 0.77 \text{ V vs. SHE} \qquad \textbf{(1)}$$

Negative electrode: $$Cr^{2+} \underset{\text{charge}}{\overset{\text{discharge}}{\rightleftharpoons}} Cr^{3+} + e^- \qquad E^0 = -0.41 \text{ V vs. SHE} \qquad \textbf{(2)}$$

Since proving unsuitable for space missions, due to low energy and power densities, the Fe-Cr RFB has seen limited research, development, and deployment efforts, at least as compared to the VRFB and despite the surge of interest in RFBs in subsequent years. This may stem from the known difficulties of operating this chemistry. Elevated temperatures (≥ 50 °C) are required in order to shift the equilibrium from the inactive Cr^{3+} complex, $[Cr(H_2O)_6]^{3+}$, to its electrochemically active counterpart, $[Cr(H_2O)_5Cl]^{2+}$ [14,18–20]. Further, the electrode potential for the Cr redox reaction is negative enough (E^o = –0.407 V vs SHE) to lead to competition with the hydrogen evolution reaction (HER), where protons are reduced to form molecular hydrogen (H_2) (E^o = 0 V vs SHE). This parasitic side reaction remains a strong impediment to the decadal operation expected for successful grid applications. Recent reports cite HER as the cause of ~1% of capacity loss per cycle for Fe-Cr RFBs [6], which is ~20× the estimated rate of capacity loss from HER in VRFBs [2]. The charge imbalance caused by this reaction also complicates electrolyte remediation protocols, necessitating additional system components to counter its impact [21,22]. Finally, the moderate OCV of 1.18 V and corrosiveness of HCl are also limiting factors, though HER mitigation has historically been the primary research focus.

While there are methods to address the HER retrospectively, using various means to correct the charge imbalance by reintroducing electrons into the system, these can complicate system operation. The simplest method is to add stoichiometric amounts of chemical reductants, as is often done for VRFBs [23,24]. This is part of the design and operating strategy proposed by Creek Channel (also referred to as “Tiger Creek” and “Cougar Creek”), a new Fe-Cr company [25]. However, over time this approach can become problematic, as the evolving H_2 gas leaves the RFB system, shifting the electrolyte pH and/or diluting the active species in the electrolyte. These effects may be further compounded by the reaction between the reductant and the electrolyte. A more complicated but arguably preferable method for rebalancing the charge is to use a secondary “recombination” cell to oxidize the generated H_2 – preferably using the species

that was oxidized against the HER reaction originally, in this case reducing Fe^{3+} to Fe^{2+} – and return these species to their original electrolytes, as has been demonstrated in several Fe-Cr systems [26,27] and, more recently, all-Fe hybrid RFB systems [28]. However, this approach adds cost and complexity to the RFB system, further reducing the appeal of researching, developing, or deploying this technology. While restoration strategies in some form may ultimately be necessary with any appreciable amount of HER, it is still desirable to minimize rates of hydrogen generation through alternative means, thus reducing the remediation costs (e.g., the number of secondary cells needed for a system is proportional to the percent of capacity lost per cycle to HER). Furthermore, facilitating longer-term operation in the absence of frequent or continuous interventions creates simplified pathways to commercialization. Indeed, the technical challenges imposed by high HER rates have seemingly impeded commercialization efforts for the Fe-Cr system, in addition to the general barriers to RFB adoption, such as limited demand for long-duration energy storage. Beyond Creek Channel (*vide supra*, a relatively newer effort), two notable prior attempts are EnerVault and Imergy (formally Deeya): the former liquidated its assets in 2015 following financial struggles [29], while the latter pivoted from Fe-Cr RFBs to VRFBs before liquidating as well [30]. In sum, the Fe-Cr RFB system poses further complications to the already stymying challenges present in VRFBs that necessitate broadly encompassing expertise in mechanical, chemical, electrochemical, and materials sciences. However, as the Fe-Cr RFB and VRFB both utilize transition metal cations in acidic supporting electrolytes and have negative redox reactions that compete with HER, many of the lessons learned from the advanced VRFB development are applicable to Fe-Cr RFBs. Accordingly, the past decade has seen renewed interest in Fe-Cr RFBs, much of which is centered on improving performance, including HER minimization. For the interested reader, a comprehensive discussion of historical Fe-Cr RFB development can be found in Reference [15].

There are many potential avenues to reduce the rate of HER [11]. One approach is to minimize local overpotentials that drive HER through electrode and/or flow field design that increase the local interfacial surface area accessible to the electrolyte. Zeng *et al.* showed improved performance in an Fe-Cr RFB using thinner electrodes (0.8 mm) and serpentine flow fields, as compared to flow-through flow fields with much thicker electrodes (6.0 mm) (although the authors of this work mainly focus on reduced ohmic and pumping losses, rather than HER suppression) [18]. Another approach is to improve the reaction selectivity, either by utilizing catalysts or tuning the electrolyte composition to promote the desired redox reactions. To this end, bismuth (Bi) has been particularly well-studied in Fe-Cr RFBs and has consistently demonstrated an ability to promote the Cr redox reaction and suppress the HER, via direct nanoparticle deposition onto the negative electrode and/or as a negative electrolyte additive [31–34]. Lead (Pb) and indium (In) have shown similar benefits as catalysts and additives [34,35]. Electrolyte composition is another avenue to address HER; beyond the use of additives, the concentrations of active species and supporting salt [36,37], as well

as choice of supporting salt, can impact HER rates [11]. For example, the recent Fe-Cr commercialization efforts by Tiger Creek (*vide supra*) claim to be utilizing a less acidic electrolyte, which could reduce HER by diminishing local proton concentrations [25], although thermodynamically-driven metal oxide formation at higher pH may challenge the implementation of milder acidic electrolytes. It should be noted, however, that catalysts and additives – particularly those based on Bi or In – can be expensive, especially if they need to be periodically replaced during the system lifetime. Finally, recent advances in ligand-complexed Fe and Cr species may enable operation in electrolytes of near-neutral pH without metal oxide formation but managing HER remains a challenge [25,38,39].

Electrolyte purification is another method to reduce HER rates by removing known catalytic precursors prior to use in a battery. Many metals are known to act as HER catalysts (e.g., copper or nickel), so their presence in the battery electrolyte, even in trace amounts, can lead to their unintended electrochemical reduction (i.e., electrodeposition) onto the negative electrode where they promote H_2 generation [11,23]. This is especially a concern in long-duration RFB systems where the ratio of electrolyte volume to electrode area is high. Purification methods include physical or chemical strategies [40], as well as electrochemical procedures that intentionally electroplate contaminants on a sacrificial electrode before the electrolyte is used in the cell of interest [41,42]. The referenced examples [40–42] are focused on or applicable to VRFB and Fe-Cr RFB systems. However, they comprise descriptions of the methodologies in the patent literature and do not demonstrate the actual impact of purification on cell performance. To our knowledge, this simple and low-cost approach of electrochemical purification has not been extensively investigated as a HER mitigation strategy in the peer-reviewed literature. In this work, we develop a protocol for electrochemical purification of the Fe-Cr negative electrolyte (shown in **Figure 1** below) and explore its effects on the cycling performance of an Fe-Cr RFB cell. We employ cyclic voltammetry to characterize unpurified and purified electrolytes, observing a marked reduction in HER activity after the electrolyte pretreatment. Next, we show that the purification process facilitates a notably reduced capacity fade rate (ca. 5× slower) during galvanostatic cycling of an Fe-Cr RFB cell, and that the effectiveness of the protocol is dependent on the relative amount of electrolyte purified. Finally, we compare the performance metrics (i.e., coulombic efficiency (CE), voltaic efficiency (VE), energy efficiency (EE), and capacity decay rate (DR)) of our cell cycling studies to those extracted from prior publications, illuminating a correlation between CE and DR. Following this trend, the performance of our cell using purified electrolyte is comparable to the performance of other cells using expensive catalysts and additives, evincing a potential cost reduction pathway for Fe-Cr RFBs.

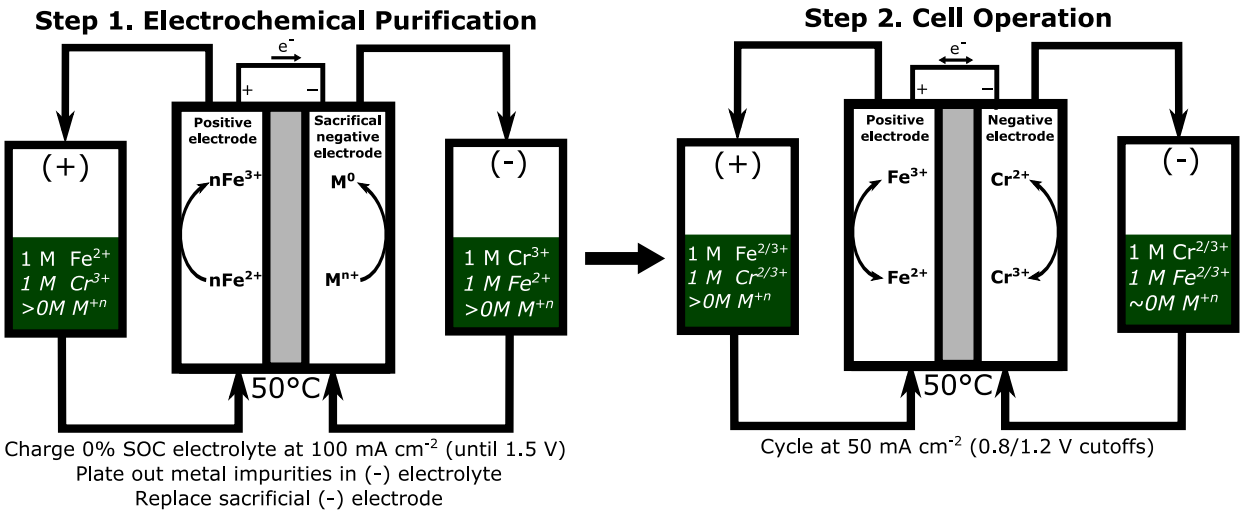

Figure 1 - Schema of the proposed electrolyte purification and cycling procedures. In Step 1, pristine 0% SOC electrolyte (1 M Fe^{2+} and 1 M Cr^{3+} in 3 M HCl, where, in each tank, the non-italicized species denote those that are intended to be redox active and the italicized species represent spectator or impurity species) is charged at 100 mA cm^{-2} (until a 1.5 V cutoff) to plate out impurities present in the negative electrolyte onto the negative electrode. The sacrificial electrode is then replaced and, in Step 2, the cell is cycled with the purified electrolyte (discharging first) at a constant current density of 50 mA cm^{-2} between 0.8 V and 1.2 V. The first charge after the initial discharge with the purified electrolyte marks the start of cycle 1 in the protocol.

Experimental Section

Cyclic voltammetry in elevated temperature – Ex situ electrochemistry was conducted in a three-electrode cell with a 3-mm diameter glassy carbon electrode (BASi), Pt coil (BASi), and Ag/AgCl in a 3 M NaCl reference electrode (BASi). The glassy carbon electrode was mirror-polished in a 0.05 μm MicroPolish alumina powder (Buehler) slurry on a microcloth disk, briefly sonicated in acetone and deionized (DI) water (Milli-Q Millipore, 18.2 MΩ cm), rinsed in DI water, and allowed to dry in air. Chromium (III) chloride hexahydrate ($CrCl_3$•$6H_2O$, ≥99.5%, Alfa Aesar, Lot No. Q16G036), iron (II) chloride tetrahydrate ($FeCl_2$•$4H_2O$, 98%, Alfa Aesar, Lot No. S18H053), and hydrochloric acid (HCl, 37%, balance of water, Sigma Aldrich) were dissolved in DI water. These species were used as received with no purification prior to experiments. The starting electrolyte was 1.0 M $FeCl_2$ / 1.0 M $CrCl_3$ in 3.0 M HCl. The procedure to generate the purified electrolyte is detailed in the *Purification Protocol* subsection of the **Experimental Section** (*vide infra*). A temperature of ca. 50 ± 5 °C was maintained by submerging a sealed vessel containing the electrodes and electrolyte into an oil bath heated by a VWR® Professional Hot Plate Stirrer with a temperature probe (VWR). Cyclic voltammograms were measured at a scan rate of 50 mV s^{-1}, starting from OCV, scanning in the positive direction to a voltage bound of 1.2 V vs Ag/AgCl, scanning in the negative direction to -1.0 V vs Ag/AgCl, and returning to the starting potential. Full *i*R-correction (100%) was employed during data acquisition by a Bio-Logic VSP potentiostat (Bio-Logic).

Heat-treatment of electrodes – Sigracet (SGL) 39AA (280 μm nominal thickness, Fuel Cell Store) electrodes were thermally oxidized in a muffle furnace (Barnstead Thermolyne Type 47900), ramping at a rate of 20 °C min^{-1} from room temperature to 500 °C, holding for 5 h, and cooling down to ambient conditions without further intervention. The electrodes were subsequently stored under air in plastic containers (McMaster-Carr). Heat-treatment conditions were chosen based on established protocols from prior literature [43–46].

Full cell RFB operation – Single-cell RFB cycling was performed in a subscale cell with a 5 cm × 5 cm (25 cm^2) active electrode area. 3× thermally-treated SGL 39AA were used for both positive and negative electrodes. The thickness of PTFE gaskets (McMaster-Carr) were selected such that the electrode stack was compressed by ca. 20%. The 5 cm × 5 cm openings in the gaskets to hold the electrodes were cut in-house. Interdigitated flow fields, milled from Tokai G347B resin-impregnated graphite plates of 3.18 mm thickness (Tokai Carbon Co.), were also employed, along with a Nafion™ 117 membrane (N117, 183 μm nominal thickness, Fuel Cell Store) presoaked in 3.0 M HCl for ≥ 24 h. The starting solution for each electrolyte (posolyte and negolyte) was 50 mL of 1.0 M $FeCl_2$ / 1.0 M $CrCl_3$ in 3.0 M HCl. Humidified nitrogen gas (Airgas, 99.999%) was bubbled through the electrolytes for > 1 h to purge residual oxygen prior to the electrochemical measurements. A flow rate of ca. 93 mL min^{-1} was maintained with a MasterFlex™ pump set at 100 rpm and circulated using LS/16 Norprene™ tubing (Cole-Parmer). The cell temperature was maintained at ca. 50 ± 5 °C using silicone adhesive-mount heating pads with a 10 W in^{-2} heating density (McMaster-Carr) connected to a benchtop PID controller (Platinum Series, CS8DPT, OMEGA Engineering), calibrated to the internal temperature of the cell components using a thermocouple probe (McMaster-Carr). The cell was cycled at a constant current density of 50 mA cm^{-2} between upper and lower cell voltage cutoffs of 1.2 V and 0.8 V, respectively, using an Arbin battery tester (FBTS-8).

Purification Protocol – To purify the negative electrolyte, the subscale cell was charged starting from 0% state-of-charge (SOC), which specifically constitutes 1.0 M $FeCl_2$ / 1.0 M $CrCl_3$ in 3.0 M HCl electrolyte in both reservoirs, at 50 °C at 100 mA cm^{-2} until a cutoff voltage of 1.5 V was reached. A potential beyond the cycling voltage cutoff of 1.2 V was set to favorably drive cathodic plating reactions on the negative electrode, thus maximizing reduction of contaminants out of solution and onto the negative electrode without over-oxidizing the positive electrode. Following the galvanostatic precharge, the electrolytes were recirculated into their respective reservoirs. The cell was then disassembled and the electrodes (negative and positive) and membrane were replaced. To avoid air ingress and self-discharge, the reservoirs remained

sealed throughout the entire process of dismantling and reassembling the cell. The purified electrolyte was discharged afterwards in the reassembled cell, and the following charge was counted as the start of the cycling protocol.

Scanning Electron Microscopy (SEM) / Energy Dispersive X-ray Spectroscopy (EDS) – SEM was performed using a Zeiss Merlin High-Resolution SEM. A 10 keV electron energy and 9.2 mm working distance with an in-lens secondary electron detector were used. Using the same acquisition parameters, energy dispersive spectroscopy (EDS) was used for elemental mapping of post-purified electrodes.

Results and Discussion

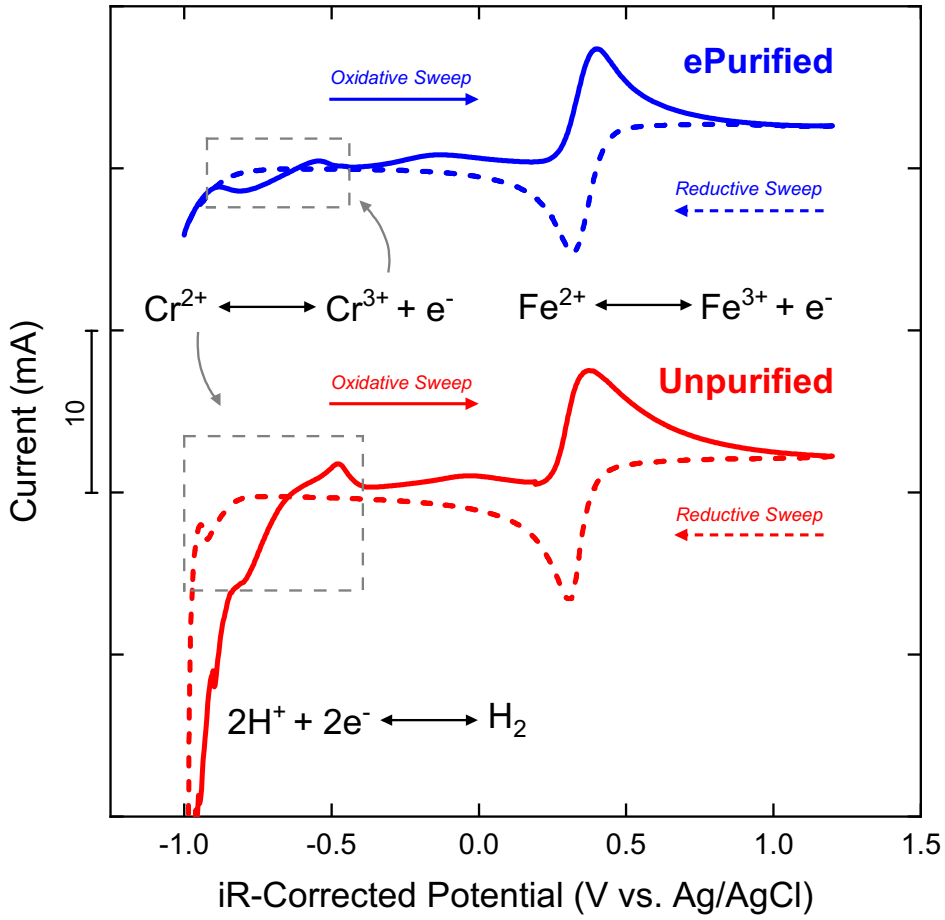

Figure 2 - Cyclic voltammograms of electrochemically purified ("ePurified," blue) and unpurified (red) electrolytes at a scan rate of 50 mV s^{-1} and a temperature of 50 °C. The unpurified electolyte composition was 1.0 M $FeCl_2$ / 1.0 M $CrCl_3$ in 3.0 M HCl. The purified electrolyte solution was harvested from the negative electrolyte reservoir of the redox flow cell after the electrochemical purification, and thus has an estimated composition of 1.0 M $FeCl_2$ / 1.0 M $CrCl_2$ in 3.0 M HCl assuming that the concentration of supporting salt and $FeCl_2$ did not change substantially during the charging, that complete conversion of Cr^{3+} to Cr^{2+} was achieved, and that deposition of the actives on the electrode did not cause significant deviations. The working, counter, and reference electrodes used were a glassy carbon disk, a Pt coil, and Ag/AgCl in 3 M NaCl.

To screen the impact of electrolyte purification on the electrolytes, we performed cyclic voltammograms (CVs) in a three-electrode cell at 50 °C. The electrolyte concentration and composition were chosen in accordance with full cell experiments. For the unpurified electrolyte, a mixed electrolyte with 1.0 M $FeCl_2$ and 1.0 M $CrCl_3$ in 3.0 M HCl was used. The purified electrolyte was collected from the negative electrolyte reservoir of an Fe-Cr RFB single cell after electrochemical purification; assuming complete reduction of Cr^{3+} to Cr^{2+} (though we posit that differences in the chromium oxidation state do not meaningfully impact the voltammetric responses), conserved supporting salt, and negligible change in Fe^{2+} concentration, the

purified electrolyte was 1.0 M $FeCl_2$ and 1.0 M $CrCl_2$ in 3.0 M HCl. The Cr redox reaction is known to be sluggish at room temperatures [38], thus requiring elevated temperatures to proceed at acceptable rates. However, H_2 readily evolves at the Cr redox potential, reducing access to catalyst sites due to bubble formation and lowering efficiencies; these side effects are exacerbated by the elevated temperatures needed to facilitate the Cr reaction.

Figure 2 shows CVs for electrochemically purified ("ePurified," blue) and unpurified (red) electrolyte conducted at a scan rate of 50 mV s^{-1}. The solid and dashed lines show the directions of oxidative and reductive sweeps, respectively. The relatively facile and reversible $Fe^{2+/3+}$ redox couple appears unchanged by the purification step, with a redox potential of ca. 0.45 V vs Ag/AgCl, in accordance with prior literature [47,48]. However, significant changes are observed with the redox events occurring at low potentials. Specifically, the untreated electrolyte demonstrates significant HER and potential contaminant deposition, evinced by the growing reductive current in the range of –0.75 V to –1.0 V vs Ag/AgCl, as compared to the lower reductive currents observed for the purified electrolyte. While, a larger Cr oxidative peak at –0.5 V vs Ag/AgCl is observed for the unpurified electrolyte in agreement with previous literature [32,36], direct comparison with the purified electrolyte is obfuscated by the large amount of visually observed H_2 bubbles formed on the preceding reductive sweep, which affects the access of solution-phase active species to the electrode surface. In contrast, both the reductive and oxidative Cr peaks are visible and discernible for the purified electrolyte, suggesting a balance between mitigating H_2 evolution while also enabling Cr and Fe redox reactions. Further, bubble formation was not observed during the CVs in the purified electrolyte. We note that Fe plating and stripping, which occurs at a standard reduction potential at –0.645 V vs Ag/AgCl, may also be a competing reaction at these negative potentials. This reaction is particularly important to mitigate, as its occurrence in the negative half-cell would catalyze HER. Altogether, the CVs suggest that H_2 evolution could be mitigated using the electrolyte purification technique.

We note that the CVs were conducted on a planar glassy carbon surface to avoid complicating the electroanalysis with porous carbon electrodes that would ultimately be used in RFB cells. Accordingly, the results for the CVs are applicable for non-heat-treated materials, enabling qualitative conclusions to be drawn for HER mitigation for only pristine carbon materials, and necessitating full-cell validation with higher-performing heat-treated electrodes that may behave differently. While the CV results are instructive, quantitative agreement between the materials sets is not anticipated, as glassy carbon surfaces are distinct from heat-treated carbon fiber surfaces due to differences in synthesis procedures, carbon allotropes, and relative degrees of surface oxidation.

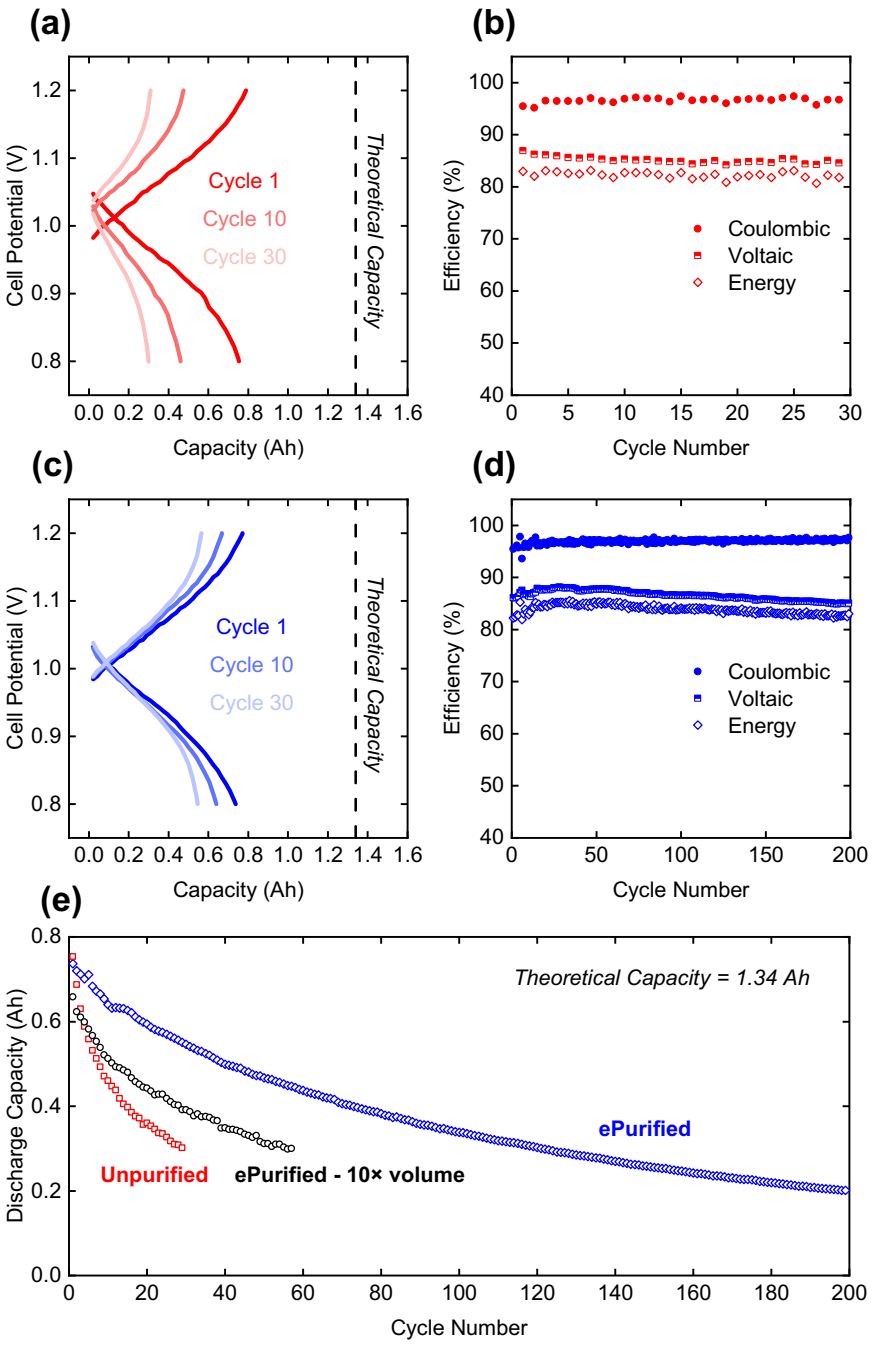

Figure 3 – Extended single-cell cycling in full Fe-Cr RFBs. (a) Potential vs capacity curves for the 1st, 10th, and 30th cycles for a full Fe-Cr RFB cell with an untreated electrolyte, and (b) corresponding coulombic, voltaic, and energy efficiencies per cycle. (c) Potential vs capacity curves for the 1st, 10th, and 30th cycles for a full Fe-Cr RFB cell with an ePurified electrolyte, and (d) corresponding coulombic, voltaic, and energy efficiencies per cycle. (e) Comparison between the discharge capacity as a function of cycle number for ePurification process on electrolyte with 50 mL volume (blue), ePurification process on electrolyte with 500 mL volume (black), and unpurified electrolyte (red). While the total volumes of electrolyte purified differed, 50 mL of electrolyte was used for cycling in all cases. All cells were cycled at a constant current density of 50 mA cm^{-2} between 0.8 and 1.2 V and at an estimated temperature of 50 °C,

with a starting electrolyte composition of 1.0 M $FeCl_2$ / 1.0 M $CrCl_3$ in 3.0 M HCl and an N117 membrane presoaked in 3.0 M HCl for ≥ 24 h. The volumetric flow rate was ca. 93 mL min^{-1}.

We evaluate the electrochemical performance of the electrochemically purified and untreated electrolyte in a single-cell Fe-Cr RFB via galvanostatic cycling at 50 mA cm^{-2} at 50 °C. An initial electrolyte composition of 1.0 M $FeCl_2$ and 1.0 M $CrCl_3$ in 3.0 M HCl was selected to match prior literature [36]. **Figure 3a** shows the voltage profiles of cycles 1, 10, and 30 for the cell with untreated electrolyte and **Figure 3b** shows the CE, VE, and EE as a function of cycle number. In comparison, **Figure 3c** shows the voltage profiles of cycles 1, 10, and 30 for the cell with ePurified electrolyte and **Figure 3d** shows the evolution of the efficiencies over 200 cycles. **Figure 3e** compares the discharge capacity as a function of cycle number for cells with electrochemical purification process on electrolyte with 50 mL volume, electrochemical purification process on electrolyte with 500 mL volume, and unpurified electrolyte. Both purified and unpurified electrolyte exhibit an initial discharge of ca. 0.74 Ah, suggesting that negligible capacity is lost to charge imbalances induced by the initial electrochemical purification (i.e., a negligible amount of Fe^{2+} in the positive electrolyte is oxidized against any of the following counter reactions in/at the negative electrolyte/electrode: metal impurity reduction, HER, or Fe cation reduction). For an electrolyte volume of 50 mL, the maximum capacity can be calculated as 1.34 Ah, indicating a 55% electrolyte utilization efficiency. While this is a modest accessed capacity, it aligns with prior reports (see **Table 1**); as such, understanding and expanding the limits of the Fe-Cr accessed capacity should be the focus of future work. A possible cause is the use of a relatively low upper voltage limit (e.g., 1.2 V) in order to minimize HER. This low initial utilization may also be due in part to only a fraction of the dissolved Cr cations being electrochemically active (i.e., in the correct Cr-speciation) [15,20,49], which is presumably why cells run at lower temperatures access even less capacity (see first row in **Table 1**). In both electrolyte conditions, the CE, VE, and EE are comparable. For the purified electrolyte, an average CE of 96.9%, average VE of 86.5%, and an average EE of 83.9% is achieved, with stable metrics for 200 cycles. For the unpurified electrolyte, an average CE of 96.9%, an average VE of 85.1%, and an average EE of 82.3% is achieved, though only for 30 cycles. The most notable difference in the cell cycling data across the two electrolytes is the reduced capacity fade rate for the purified electrolyte compared to the untreated electrolyte, as evinced by the slower decay in the discharge capacity as a function of cycle number (**Figure 3e**). We posit that the discrepancy in capacity fade despite nearly identical efficiencies is due to chemical reactions between the active materials and impurities (e.g., Cr^{2+} reducing impurity metal cations) or the active materials and the supporting salt and solvent (e.g., H_2 generation due to solution-phase charge-transfer in the negative electrolyte) [50], since these reactions do not directly impact the measured efficiencies. There may also be capacity losses from HER evolved on charge from impurities in the unpurified electrolyte, as these efficiencies are relative measures of losses for individual cycles, and are unable to capture losses between

cycles. To quantify the DR, we determine the number of cycles at which 50% of the maximum discharge capacity utilization (i.e., 0.37 Ah) is reached to avoid effects of non-linear fade at later cycles. The steeper initial capacity drop may be a consequence of diminishing activity of the oxygen groups on the electrode formed during oxidative pretreatment that occurs as the electrode undergoes prolonged cycling and whose deactivation is more pronounced for the Cr reaction due to its lower redox potential [51]. The untreated electrolyte reaches the cutoff within 17 cycles (13.9 h total duration), while the purified electrolyte operates for 87 cycles (71.7 h total duration) prior to reaching the same capacity retention. This corresponds to DRs of 2.94 % / cycle and 0.57 % / cycle for the first 50 cycles for the unpurified and purified electrolytes, respectively. We note that our own efforts to rebalance spent electrolytes by mixing the used positive and negative electrolytes together, dividing the mixed electrolyte into two equal volumes, and resuming operation did not lead to significant capacity recovery, suggesting that the mechanisms of capacity fade were not predominantly due to species crossover. The same purification protocol was performed with 10× the original electrolyte volume to evaluate its effectiveness as a function of volume to be purified. The same total electrolyte volume of 50 mL was taken from the larger volume of purified electrolyte and cycled. **Figure 3e** shows that while capacity fade was mitigated compared to no treatment, it is more rapid than with a smaller volume of purified electrolyte. One possible explanation is that not all the electrolyte impurities are removed with the larger volume of electrolyte if purified using the same reactor size (i.e., there is not enough electrode surface area to plate out all the metal impurities present in the larger electrolyte volume). This hypothesis implies there is, perhaps, a ratio of electrolyte volume to electrode surface area that cannot be exceeded for sufficient purification or operation; quantification and optimization of such a ratio should be the focus of future work.

We seek to contextualize our results within the broader set of efforts made to alleviate capacity fade in Fe-Cr RFBs. Summaries of performance metrics from a non-exhaustive list of prior literature is summarized in **Table 1**. Some of the data is adapted in part from the recent review by Sun and Zhang [15]. Approximate averages for the CE, VE, and EE of longer-duration galvanostatic cycling tests are shown, along with estimated discharge capacity decay per cycle. Self-reported data were used whenever possible; if the capacity DR was not reported, the DR to 50% of the original capacity was extracted from published figures. The use of different electrode materials and thicknesses, electrolyte compositions, flow field designs, in-house cell architectures, laboratory practices, and cycling parameters stymy exact comparison of the approaches used across the literature. Thus, we include operating conditions and parameters used (i.e., electrode materials with geometric dimensions, flow fields, membrane, electrolyte concentrations and volumes). Notably, most strategies to improve the performance in Fe-Cr RFBs rely on materials advances, including membrane design, electrocatalyst development, or electrolyte additives, all designed to suppress mechanisms of capacity fade (e.g., HER and crossover). To the best of our knowledge, none of these studies

refer to specific procedures to activate or purify electrolytes prior to electrochemical evaluation, beyond increasing the operating temperature. Furthermore, there appears to be no discussion or consensus on the standard grade of chemicals or specific vendors needed to uphold baseline cell performance. Our approach to electrochemically purify electrolytes results in comparable CE, VE, EE, and DR to values reported in existing literature.

Table 1 – Summary of performance metrics from select, recent Fe-Cr RFB literature used to construct **Figure 4**. Electrode and flow–field combinations, membrane type, and electrolyte compositions are reported, along with corresponding performance metrics of longer-duration galvanostatic cycling of the cells. These consist of the approximate averages for the coulombic efficiency (CE), voltaic efficiency (VE), energy efficiency (EE), and estimated discharge capacity decay rate per cycle. Self-reported data were used whenever possible. If the capacity decay rate was not reported, the decay rate to 50% of the original capacity was extracted from published graphs. Otherwise, the reported decay rate was used, even if it was not to 50% of the original value, as the reported value is expected to be more accurate than the extracted values. We elected to report our decay rate in terms of decay rate to 50% of the original discharge capacity. Chart format and values adapted in part from Reference [15].

Referenced Work	Electrode / Flow Field / Active Area / Uncompressed Electrode Thickness	Membrane	Electrolyte / Temperature / Volume	Current Density (mA cm^{-2})	CE (%)	VE (%)	EE (%)	Capacity Decay Rate* (% / cycle)	Maximum Discharge Capacity / Theoretical Discharge Capacity (Ah/L)	Theoretical Accessible Capacity on Cycle 1 (%)	Ref.
Ahn & Moon *et al.*, 2021	Carbon Felt + Bi-C electrocatalyst / Flow-type / 2.0 × 3.0 cm^2 / 4.3 mm	Nafion 117	1.2 M $FeCl_2$ + 1.5 M $CrCl_3$ in 2.0 M HCl / Room Temperature / 20 mL	40	97.4	88.5	86.2	0.50	9.2 / 32.2	28.6	[31]
	Carbon Felt + KB / Flow-type / 2.0 × 3.0 cm^2 / 4.3 mm			40	97.2	82.2	79.9	0.637	9.1 / 32.2	28.3	
	Carbon Felt / Flow-type / 2.0 × 3.0 cm^2 / 4.3 mm			40	96	72.8	69.9	0.883	8.08 / 32.2	25.1	
Chen *et al*., 2020	Silicic acid etched 500 °C for 5 h Graphite Felt / Flow-through / 3.0 × 3.0 cm^2 / 5 mm	Nafion 115	1.0 M $FeCl_2$ + 1.0 M $CrCl_3$ in 3.0 M HCl / 65 °C / 50 mL	120	92.4	86.3	79.7	0.46	14.60 / 26.8	54.5	[43]
	500 °C for 5 h Graphite Felt / Flow-through / 3.0 × 3.0 cm^2 /			120	96.4	74.1	71.4	1.16	11.68 / 26.8	43.6	

	5 mm										
Sun *et al*., 2019	500 °C for 5 h Graphite Felt / Flow-type / 3.0 × 3.0 cm^2 / 5 mm	SPEEK (sulfonated poly(ether ether ketone)	1.0 M $FeCl_2$ + 1.0 M $CrCl_3$ in 3.0 M HCl / 65 °C / 50 mL	80	98.5	80.3	79.1	0.84	-- / 26.8	--	[44]
		Nafion 115		80	96.0	85.7	82.3	1.56	-- / 26.8		
Zhang *et al*., 2019	Graphite Felt / Flow-through / 3.0 × 3.0 cm^2 / 6.25 mm	Nafion 115	1.0 M $FeCl_2$ + 1.0 M $CrCl_3$ in 3.0 M HCl / 65 °C / 50 mL	60	93.1	81.8	76.1	1.19	-- / 26.8	--	[52]
Zhang *et al*., 2020	500 °C for 5 h Graphite Felt / Flow-through / 3.0. × 3.0 cm^2 / 5 mm	Nafion 115	1.0 M $FeCl_2$ + 1.0 M $CrCl_3$ in 3.0 M HCl + 8 mM $BiCl_3$ / 65 °C / 50 mL	60	96.9	89	86.3	1.2	-- / 26.8	--	[45]
	Graphite Felt / Flow-through / 3.0 × 3.0 cm^2 / 5 mm			60	94.3	91.7	86.4	2.9	-- / 26.8	--	
	500 °C for 5 h Carbon Felt / Flow-through / 3.0 × 3.0 cm^2 / 5 mm			60	95.9	83.7	80.3	1.26	-- / 26.8	--	
	Carbon Felt / Flow-through / 3.0 × 3.0 cm^2 / 5 mm			60	84.9	80.6	63.3	2.99	-- / 26.8	--	
Zeng *et al*., 2015	400 °C for 6 h Graphite Felt / Flow-through / 2.0 × 2.5 cm^2 / 6 mm	Nafion 212	1.0 M $FeCl_2$ + 1.0 M $CrCl_3$ in 3.0 M HCl + 0.01 M Bi^{3+} (Bi_2O_3) / 65 °C / 20 mL	80	96.2	85.8	82.5	1.2	-- / 26.8	--	[6]
Zeng *et al*., 2016	Mixed acid-boiled Carbon Paper / Flow-Field Structured / 2.0 × 2.0 cm^2 / 0.8 mm	Nafion 212	1.0 M $FeCl_2$ + 1.0 M $CrCl_3$ in 3.0 M HCl + 0.005 M Bi^{3+} (Bi_2O_3) / 65 °C / 20 mL	160	97.4	85.1	82.9	0.6	-- / 26.8	--	[18]
Zeng *et al*., 2016	500 °C for 5 h Carbon Paper / Interdigitated Flow-Field (IDFF) / 2.0 × 2.0 cm^2 / 0.8 mm	Nafion 212	1.0 M $FeCl_2$ + 1.0 M $CrCl_3$ in 3.0 M HCl + 0.005 M Bi^{3+} (Bi_2O_3) / 65 °C / 20 mL	320	97.8	81.5	79.7	0.5	-- / 26.8	--	[46]
Wang *et al*., 2021	Graphite Felt / Flow-through / 5.0 × 10.0 cm^2 / 5.3 mm	Perfluorosulfonic-acid ion exchange membrane	1.0 M $FeCl_2$ + 1.0 M $CrCl_3$ in 3.0 M HCl + 0.01 M $InCl_3$ / 65 °C / 70 mL	160	98.2	80.1	78.7	0.16	18.7 / 26.8	69.8	[35]
			1.0 M $FeCl_2$ + 1.0 M $CrCl_3$ in	160	97.2	80.1	77.9	0.42	18.6 / 26.8	69.3	

			3.0 M HCl / 65 °C / 70 mL								
This work: ePurified	500 °C for 5 h Carbon Paper / IDFF / 5.0 × 5.0 cm^2 / 0.84 mm	Nafion 117	1.0 M $FeCl_2$ + 1.0 M $CrCl_3$ in 3.0 M HCl / 50 °C / 50 mL	*50*	*96.9*	*86.5*	*83.9*	*0.57*	*14.8 / 26.8*	*55.0*	--
This work: Unpurified	500 °C for 5 h Carbon Paper / IDFF / 5.0 × 5.0 cm^2 / 0.84 mm	Nafion 117	1.0 M $FeCl_2$ + 1.0 M $CrCl_3$ in 3.0 M HCl / 50 °C / 50 mL	*50*	*96.6*	*85.1*	*82.3*	*2.94*	*15.1 / 26.8*	*56.2*	--

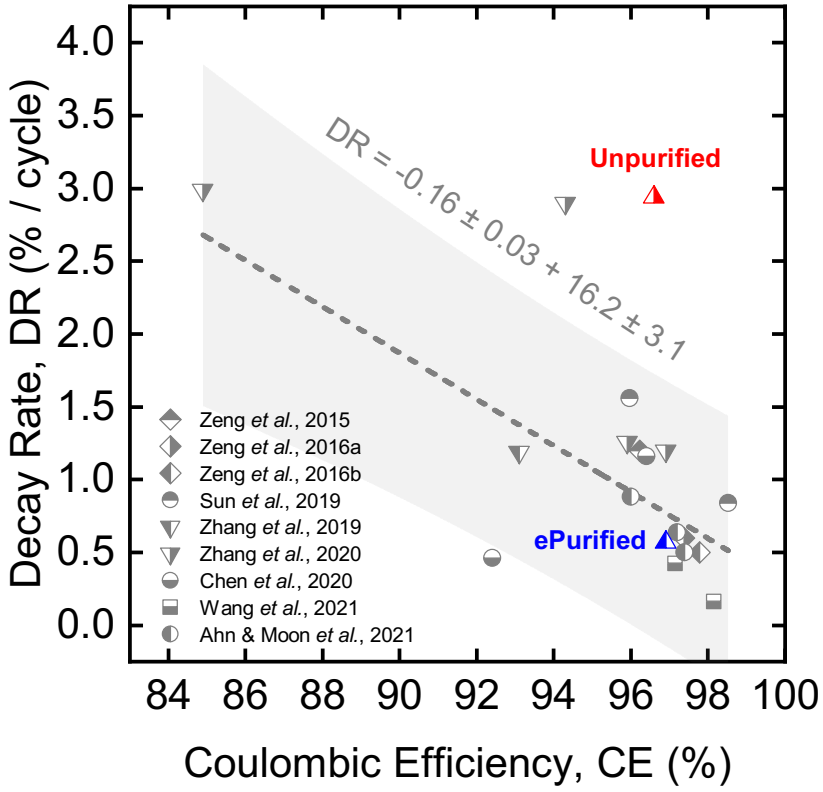

Figure 4 – Decay rate of discharge capacity as a function of average coulombic efficiency. Unpurified electrolyte (red triangle) and purified electrolyte (blue triangle) from this work are shown amid other performance metrics reported in the Fe-Cr RFB literature. The gray dotted trendline is the ordinary least squares fit of the data excluding the unpurified electrolyte and the outlier from Zhang *et al.* (2020) [45].

We hypothesized that DR may be associated with CE, as CE is an indicator of unmatched capacity across subsequent discharge and charge half cycles and we anticipate an important contributor to the DR is HER. The statistical significance of the association between CE and DR was confirmed using the Kendall rank correlation analysis between seven variables (electrode thickness, geometric area, current density rate, CE,

VE, EE, and DR) [53]. These results are shown in **Figure S1** and further details on the statistical basis of the Kendall analysis can be found in the **Supporting Information**. As noted above, the presence of soluble mediators can also contribute to the H_2 generation in Fe-Cr RFBs (i.e., charge-transfer in solution) [50], although determining the extent and identity of these exchanges is beyond the scope of the present analysis. We explore the relationship between DR and CE in **Figure 4** plotting data harvested from the published literature on Fe-Cr RFBs along with our own results for the purified and unpurified electrolytes. Despite all of the aforementioned differences in experimental conditions and HER mitigation strategies, we observe a linear negative trend between DR and CE, whereby higher CE generally correlates to lower DR. We note the existence of two points considered to be outliers; a cell with unpurified electrolyte from our own report (this study), and a cell using pristine graphite felt from Zhang *et al.* (2020) [45]. These two data points exhibit comparatively high DR despite high CE. Excluding these two points, we identify ordinary least squares fit to the DR versus CE data. These values, however, are to be taken semi-quantitatively, as sources of error including ranging current densities, cycle numbers, and inaccuracies from self-reporting; thus, we plot a 95% prediction band to accompany the line-of-best-fit. Further, we note that while the relationship between DR and CE is expected to be negatively correlated, the precise nature of the relationship is likely more nuanced due to convoluting factors such as species crossover rates and non-linear effects that vary with operating conditions. Nevertheless, our electrochemical purification protocol falls near the fitted trendline towards the higher end of the reported CEs, suggesting that this strategy can have a similarly beneficial effect on cell performance as approaches in electrocatalyst design and electrolyte additives.

In order to explain the two outliers in **Figure 4**, one may consider the interaction of three key factors: 1) total surface area of the electrodes (especially the negative electrodes), 2) how easily-reducible impurities in the electrolyte can impact the cell performance and the electrolyte composition, and 3) how the addition of Bi can impact both the cell performance and the impact of impurities. The impact on VE and CE on each of these factors, independently, is summarized in **Table 2**. Most of the cells summarized in **Table 1** use porous electrodes with high interfacial-to-geometric surface area ratios, as they use thick carbon felts that have been thermally treated. In all of these cases, the impact of impurities on the cell performance should be significantly reduced relative to electrodes with lower interfacial-to-geometric surface ratios since the resulting impurity density on the negative electrode is concomitantly lower. The two outliers identified previously can be explained primarily by their electrode surface areas. Our work uses carbon papers that are significantly thinner than felts and have specific surface areas on the order of 5 – 20 $m^2\ g^{-1}$ (based on previous reports on the surface areas of heat-treated paper electrodes) [54,55]. The pristine felt electrodes used in Zhang 2020 [45] have surface areas that are ca. 6× lower than when they have been thermally oxidized (e.g., the reported BET surface areas are < 2 and 9-14 $m^2\ g^{-1}$ for pristine and thermally pretreated felts, respectively). In the other cases that use carbon papers [46,56] or untreated felt electrodes [31,45], Bi

cations are added to the electrolyte, which will presumably compete or co-deposit with reducible impurities in the electrolyte. The result is lower amounts of and attenuated effects from reduced impurities deposited on the negative electrodes, and thus high CEs and low DRs. Unfortunately, the impact of impurities for all of the cases summarized in **Table 1** is limited to qualitative comparisons, as most publications do not report electrolyte chemical purities. Even if these values were reported, it would not be sufficient, since impurity speciation would also need to be known for a quantitative assessment of the impact.

Table 2. The expected impact on VE and CE of three key factors.

	Higher total electrode surface area	**Impurities that can readily be reduced at the negative electrode**	**Addition of Bi catalysts**
Impact on VE	Higher, due to lower reaction turnover rates per actual area at a given operating geometric current density	None expected	Higher, due to reduced overpotential on the negative electrode
Impact on CE	Indirectly higher*, due to reduced overpotentials	None or Lower**	Indirectly higher*, due to reduced overpotentials on the negative electrode
Interactions	Lower density of reduced impurities (and Bi, if present) per actual area	Less impact with higher surface area electrodes or with the addition of Bi	Lower density and attenuated HER from reduced impurities since Bi counteracts effects of impurities on negative electrodes

* The relation is indirect under the assumption that the reduced overpotential enabled by the factor encourages operation at higher current density, and thus higher CE.
** None, if the impurities are reduced in electrolyte. Lower, if the impurities act as HER catalysts.

To investigate the origin of the deposited species during electrochemical purification, we performed scanning electron microscopy (SEM) and energy dispersive X-ray spectroscopy (EDS) on the negative electrodes used in the purification step comparing the results to those of an unexposed heat-treated SGL 39AA electrode (see **Figure S2** in the **Supporting Information**). While the SEM / EDS revealed that the negative electrode used in the purification process exhibited Fe, Cr, and chlorine signals in addition to carbon and oxygen species and trace silicon from the electrode, it remains difficult to pinpoint the precise phases of the plated contaminants without a more detailed spectroscopic analysis. Although we hypothesize that the effect of high concentrations of active species and impurities from various sources are mitigated when first subjected to the electrochemical purification step, we also posit that the impurity concentrations

are relatively low and thus are difficult to detect, but have non-negligible effects on cell performance, as discharge capacity decay rate is dependent on the amount of purified electrolyte volume as a function of electrode surface area (**Figure 3e**). If these impurities act as HER catalysts, only a small amount is required to have a significant impact as shown in the CVs in **Figure 2**. Further studies leveraging more precise *in situ* or *ex situ* spectroscopy will prove valuable to ascertain the chemical identities of the deposited impurities. Additionally, broader efforts to systematically quantify the purities of component chemicals and their resulting electrolyte solutions may lend valuable insight for future development campaigns.

Conclusion

Hydrogen-evolution mitigation strategies in Fe-Cr RFB systems have largely focused on materials and reactor design innovation. These techniques can add cost and complexity, particularly approaches that utilize expensive metals (e.g., Bi, In) as catalysts on the electrode or additives in the electrolyte. Here, we demonstrate an alternative, potentially low-cost approach to mitigate HER: electrochemical electrolyte purification. We demonstrate that this strategy leads to significant reduction in capacity fade at appreciable current density over extended cycling experiments and produces results that are on-par with literature that teach materials-centric strategies. We hypothesize that the purification process reduces and filters out metal impurities that can react with the active materials or catalyze deleterious hydrogen generation on the negative electrode lowering accessible capacity over time. Importantly, this purification process does not appear to induce a significant charge imbalance that would, in itself, reduce the accessible capacity. We show that a clear association between discharge capacity decay rate and coulombic efficiency exists based on durational cycling data obtained from the peer-reviewed literature, and that our cell data with electrochemically purified electrolyte falls well within that trend, although our cell data with unpurified electrolyte demonstrates an abnormally high decay rate at moderate coulombic efficiency. The connection between coulombic efficiency and decay rate semi-quantitatively elucidates the importance of attenuating HER attempted through numerous strategies for more resilient Fe-Cr RFBs.

Future work should explore the universality of the strategy across materials sets (i.e., electrolytes of varying purity levels, electrodes of different formats), operating conditions (i.e., temperatures, flow rates), and related electrochemical purification approaches (i.e., potentials holds, different potential cutoffs), in tandem with precise methods for impurity detection. Finally, despite the improvements realized through electrolyte purification, the cell performance remains poor: total accessed capacity, even during the first cycle, is limited (~60%) and discharge capacity decay rate is rapid (e.g., ≈ 50% in approximately 100 cycles), indicating high rates of irreversible capacity loss persist (as the discharge capacity was not recoverable via

electrolyte rebalancing). Concerted research efforts are needed to understand and control the fundamental processes that govern the performance and longevity of Fe-Cr RFBs.

CReDIT authorship contribution statement

Charles Tai-Chieh Wan: Conceptualization, Methodology, Software, Validation, Formal Analysis, Investigation, Data Curation, Writing – Original Draft, Writing – Review & Editing, Visualization. **Kara E. Rodby:** Conceptualization, Methodology, Software, Validation, Formal Analysis, Investigation, Data Curation, Writing – Original Draft, Writing – Review & Editing, Visualization. **Mike L. Perry:** Conceptualization, Methodology, Investigation, Writing – Original Draft, Writing – Review & Editing. **Yet-Ming Chiang:** Funding Acquisition. **Fikile R. Brushett:** Conceptualization, Writing – Original Draft, Writing – Review & Editing, Project administration.

Acknowledgments

The authors acknowledge the support from MIT's Center for Materials Science and Engineering Shared Experimental Facilities, supported in part by the MRSEC Program of the National Science Foundation under Award No. DMR1419807. Research by C.T.W., Y.M.C., and F.R.B. was supported by the Joint Center for Energy Storage Research (JCESR), an Energy Innovation Hub funded by the U.S. Department of Energy, Office of Science, Basic Energy Sciences. C.T.W. acknowledges a graduate fellowship through the National Science Foundation Graduate Research Fellowship Program under Grant No. 1745302. Any opinions, findings, and conclusions or recommendations expressed in this material are those of the authors and do not necessarily reflect the views of the National Science Foundation. We appreciate the collaborative efforts of the Raytheon Technologies Research Center, specifically for supplying the 25 cm^2 flow cell employed in this study.

References

[1] US Department of Energy, DOE OE Global Energy Storage Database, (2020). https://www.sandia.gov/ess-ssl/global-energy-storage-database-home/ (accessed January 10, 2020).

[2] K.E. Rodby, T.J. Carney, Y. Ashraf Gandomi, J.L. Barton, R.M. Darling, F.R. Brushett, Assessing the levelized cost of vanadium redox flow batteries with capacity fade and rebalancing., Journal of Power Sources. 460 (2020) 227958. https://doi.org/10.1016/j.jpowsour.2020.227958.

[3] M.L. Perry, J.D. Saraidaridis, R.M. Darling, Crossover Mitigation Strategies for Redox-Flow Batteries, Current Opinion in Electrochemistry. 21 (2020) 311–318. https://doi.org/10.1016/j.coelec.2020.03.024.

[4] R.A. Potash, J.R. McKone, S. Conte, H.D. Abruña, On the Benefits of a Symmetric Redox Flow Battery, Journal of The Electrochemical Society. 163 (2016) A338–A344. https://doi.org/10.1149/2.0971602jes.

[5] M.-A. Goulet, M.J. Aziz, Flow Battery Molecular Reactant Stability Determined by Symmetric Cell Cycling Methods, Journal of The Electrochemical Society. 165 (2018) A1466–A1477. https://doi.org/10.1149/2.0891807jes.
[6] Y.K. Zeng, T.S. Zhao, L. An, X.L. Zhou, L. Wei, A comparative study of all-vanadium and iron-chromium redox flow batteries for large-scale energy storage, Journal of Power Sources. 300 (2015) 438–443. https://doi.org/10.1016/j.jpowsour.2015.09.100.
[7] Vanadium Price, (2021). https://www.vanadiumprice.com/ (accessed November 8, 2021).
[8] US Department of Energy, Grid Energy Storage, 2013.
[9] ARPA-E, ARPA-E: The First Seven Years, 2016.
[10] K.E. Rodby, M.L. Perry, F.R. Brushett, Assessing capacity loss remediation methods for asymmetric redox flow battery chemistries using levelized cost of storage, Journal of Power Sources. 506 (2021) 230085. https://doi.org/10.1016/j.jpowsour.2021.230085.
[11] M.L. Perry, K.E. Rodby, F.R. Brushett, Untapped Potential: The Need and Opportunity for High-Voltage Aqueous Redox Flow Batteries, ACS Energy Letters. (2022) 659–667. https://doi.org/10.1021/acsenergylett.1c02225.
[12] US Geological Survey, Mineral Commodity Summaries 2020, 2020.
[13] R.F. Schulte, B.N. Bryden, Mineral Industry Surveys: Chromium December 2020, 2020.
[14] R. Gahn, N. Hagedorn, J. Ling, Single Cell Performance Studies on the Fe / Cr Redox Energy Storage System Using Mixed Reactant Solutions at Elevated Temperature Conservation and Renewable Energy Division of Energy Storage Systems, Proceedings of the Eighteenth Intersociety Energy Conversion Engineering Conference, Orlando, FL, August 21-26, 1983. Volume 4. (1983) 1647–1652.
[15] C. Sun, H. Zhang, Review of the Development of First-Generation Redox Flow Batteries: Iron-Chromium System, ChemSusChem. (2021). https://doi.org/10.1002/cssc.202101798.
[16] Y.S. Kim, S.H. Oh, E. Kim, D. Kim, S. Kim, C.H. Chu, K. Park, Iron-chrome crossover through nafion membrane in iron-chrome redox flow battery, Korean Chemical Engineering Research. 56 (2018) 24–28. https://doi.org/10.9713/kcer.2018.56.1.24.
[17] B. Hu, J. Luo, C. DeBruler, M. Hu, W. Wu, T.L. Liu, Redox-Active Inorganic Materials for Redox Flow Batteries, in: H. Wang, B.P.T. Fokwa (Eds.), Inorganic Battery Materials, Wiley, 2019: pp. 211–236.
[18] Y.K. Zeng, X.L. Zhou, L. An, L. Wei, T.S. Zhao, A high-performance flow-field structured iron-chromium redox flow battery, Journal of Power Sources. 324 (2016) 738–744. https://doi.org/10.1016/j.jpowsour.2016.05.138.
[19] R.F. Gahn, N.H. Hagedorn, J.A. Johnson, Cycling Performace of the Iron- Chromium Redox Energy Storage System Conservation and Renewable Energy, Nasa Tm-87034. (1985).
[20] D.A. Johnson, M.A. Reid, Chemical and Electrochemical Behavior of the Cr(III)/Cr(II) Half-Cell in the Iron-Chromium Redox Energy Storage System, J. Electrochem. Soc. 132 (1985) 1058. https://doi.org/10.1149/1.2114015.
[21] O.K. Chang, A.Q. Pham, Rebalancing electrolytes in redox flow battery systems, 8,916,281 B2, 2014.
[22] K. Wei, L. Li, Fe-Cr redox flow battery systems including a balance arrangement and methods of manufacture and operation, 10,777,836 B1, 2020.
[23] L. Cao, M. Skyllas-Kazacos, C. Menictas, J. Noack, A review of electrolyte additives and impurities in vanadium redox flow batteries, Journal of Energy Chemistry. 27 (2018) 1269–1291. https://doi.org/10.1016/j.jechem.2018.04.007.
[24] R.M. Darling, M.L. Perry, Method of maintaining health of flow battery, 20160056487 A1, 2013.
[25] L. LI, Q. Luo, Near Neutral Aqueous Fe-Cr Complex Flow Battery: Reducing Electricity Storage Cost to < $100/kWh, ECS Meeting Abstracts. MA2021-02 (2021) 120–120. https://doi.org/10.1149/MA2021-021120mtgabs.

[26] Y.K. Zeng, T.S. Zhao, X.L. Zhou, J. Zou, Y.X. Ren, A hydrogen-ferric ion rebalance cell operating at low hydrogen concentrations for capacity restoration of iron-chromium redox flow batteries, Journal of Power Sources. 352 (2017) 77–82. https://doi.org/10.1016/j.jpowsour.2017.03.125.
[27] R.F. Gahn, Method and apparatus for rebalancing a redox flow cell system, 4,576,878, 1986.
[28] Y. Song, C.E. Evans, Method and system for rebalancing electrolytes in a redox flow battery system, 10,923,753, 2021.
[29] E. Wessof, Flow Battery Startup EnerVault Files for Assignment Before Creditors, (2015). https://www.greentechmedia.com/articles/read/Flow-Battery-Startup-EnerVault-Files-For-Assignment-Before-Creditors (accessed January 25, 2022).
[30] E. Wesoff, Flow Battery Aspirant Imergy Has Let Go Its Staff and Is Selling Its Assets, (2016). https://www.greentechmedia.com/articles/read/flow-battery-aspirant-imergy-has-let-go-its-staff-and-is-selling-its-assets (accessed January 25, 2022).
[31] Y. Ahn, J. Moon, S.E. Park, J. Shin, J. Wook Choi, K.J. Kim, High-performance bifunctional electrocatalyst for iron-chromium redox flow batteries, Chemical Engineering Journal. (2021) 127855. https://doi.org/10.1016/j.cej.2020.127855.
[32] Y.K. Zeng, T.S. Zhao, X.L. Zhou, L. Zeng, L. Wei, The effects of design parameters on the charge-discharge performance of iron-chromium redox flow batteries, Applied Energy. 182 (2016) 204–209. https://doi.org/10.1016/j.apenergy.2016.08.135.
[33] H. Zhang, Y. Tan, J. Li, B. Xue, Studies on properties of rayon- and polyacrylonitrile-based graphite felt electrodes affecting Fe/Cr redox flow battery performance, Electrochimica Acta. 248 (2017) 603–613. https://doi.org/10.1016/j.electacta.2017.08.016.
[34] S.R. Tirukkovalluri, R.K. Hanuman Gorthi, Synthesis, characterization and evaluation of Pb electroplated carbon felts for achieving maximum efficiency of Fe-Cr redox flow cell, Journal of New Materials for Electrochemical Systems. 16 (2013) 287–292. https://doi.org/10.14447/jnmes.v16i4.155.
[35] S. Wang, Z. Xu, X. Wu, H. Zhao, J. Zhao, J. Liu, C. Yan, X. Fan, Excellent stability and electrochemical performance of the electrolyte with indium ion for iron–chromium flow battery, Elsevier Ltd, 2021. https://doi.org/10.1016/j.electacta.2020.137524.
[36] S. Wang, Z. Xu, X. Wu, H. Zhao, J. Zhao, J. Liu, C. Yan, X. Fan, Analyses and optimization of electrolyte concentration on the electrochemical performance of iron-chromium flow battery, Applied Energy. 271 (2020) 115252. https://doi.org/10.1016/j.apenergy.2020.115252.
[37] M. Lopez-Atalaya, G. Codina, J.R. Perez, J.L. Vazquez, A. Aldaz, Optimization studies on a Fe/Cr redox flow battery, Journal of Power Sources. 39 (1992) 147–154. https://doi.org/10.1016/0378-7753(92)80133-V.
[38] B.H. Robb, J.M. Farrell, M.P. Marshak, Chelated Chromium Electrolyte Enabling High-Voltage Aqueous Flow Batteries, Joule. 3 (2019) 2503–2512. https://doi.org/10.1016/j.joule.2019.07.002.
[39] S.E. Waters, B.H. Robb, M.P. Marshak, Effect of Chelation on Iron–Chromium Redox Flow Batteries, ACS Energy Lett. 5 (2020) 1758–1762. https://doi.org/10.1021/acsenergylett.0c00761.
[40] M. Keshavarz, A. Varadarajan, Preparation of flow cell battery electrolytes from raw materials, US 8,394,529 B2, 2013.
[41] J.T. Sullivan, Electrochemical-based purification of electrolyte solutions, and related systems and methods, US 10333164, 2019.
[42] Z.M. Norman, A.B. Papandrew, R.C. Klet, M. Millard, Methods and devices for removing impurities from electrolytes, WO 2020/086645 A1, 2020.
[43] N. Chen, H. Zhang, X.-D. Luo, C.-Y. Sun, SiO2-decorated graphite felt electrode by silicic acid etching for iron-chromium redox flow battery, Electrochimica Acta. 336 (2020) 135646. https://doi.org/10.1016/j.electacta.2020.135646.
[44] C.-Y. Sun, H. Zhang, X.-D. Luo, N. Chen, A comparative study of Nafion and sulfonated poly(ether ether ketone) membrane performance for iron-chromium redox flow battery, Ionics. 25 (2019) 4219–4229. https://doi.org/10.1007/s11581-019-02971-0.

[45] H. Zhang, N. Chen, C. Sun, X. Luo, Investigations on physicochemical properties and electrochemical performance of graphite felt and carbon felt for iron-chromium redox flow battery, International Journal of Energy Research. 44 (2020) 3839–3853. https://doi.org/10.1002/er.5179.
[46] Y.K. Zeng, X.L. Zhou, L. Zeng, X.H. Yan, T.S. Zhao, Performance enhancement of iron-chromium redox flow batteries by employing interdigitated flow fields, Journal of Power Sources. 327 (2016) 258–264. https://doi.org/10.1016/j.jpowsour.2016.07.066.
[47] J. Friedl, U. Stimming, Determining Electron Transfer Kinetics at Porous Electrodes, Electrochimica Acta. 227 (2017) 235–245. https://doi.org/10.1016/j.electacta.2017.01.010.
[48] M.H. Gharahcheshmeh, C.T.-C. Wan, Y.A. Gandomi, K.V. Greco, A. Forner-Cuenca, Y.-M. Chiang, F.R. Brushett, K.K. Gleason, Ultrathin Conformal oCVD PEDOT Coatings on Carbon Electrodes Enable Improved Performance of Redox Flow Batteries, Advanced Materials Interfaces. 7 (2020) 2000855. https://doi.org/10.1002/admi.202000855.
[49] D.Sh. Cheng, A. Reiner, E. Hollax, Activation of hydrochloric acid-CrCl3 · 6H2 solutions with N-alkyfamines, J Appl Electrochem. 15 (1985) 63–70. https://doi.org/10.1007/BF00617741.
[50] Z.P. Ifkovits, J.M. Evans, M.C. Meier, K.M. Papadantonakis, N.S. Lewis, Decoupled electrochemical water-splitting systems: a review and perspective, Energy Environ. Sci. 14 (2021) 4740–4759. https://doi.org/10.1039/D1EE01226F.
[51] E. Hollax, D.Sh. Cheng, The influence of oxidative pretreatment of graphite electrodes on the catalysis of the Cr3+Cr2+ and Fe3+Fe2+ redox reactions, Carbon. 23 (1985) 655–664. https://doi.org/10.1016/0008-6223(85)90225-8.
[52] H. Zhang, Y. Tan, X. Luo, C. Sun, N. Chen, Polarization Effects of a Rayon and Polyacrylonitrile Based Graphite Felt for Iron-Chromium Redox Flow Batteries, ChemElectroChem. 6 (2019) 3175–3188. https://doi.org/10.1002/celc.201900518.
[53] M.G. Kendall, Rank correlation methods, Griffin, Oxford, England, 1948.
[54] K.V. Greco, A. Forner-Cuenca, A. Mularczyk, J. Eller, F.R. Brushett, Elucidating the Nuanced Effects of Thermal Pretreatment on Carbon Paper Electrodes for Vanadium Redox Flow Batteries, ACS Appl. Mater. Interfaces. 10 (2018) 44430–44442. https://doi.org/10.1021/acsami.8b15793.
[55] K.V. Greco, J.K. Bonesteel, N. Chanut, C. Tai-Chieh Wan, Y.-M. Chiang, F.R. Brushett, Limited accessibility to surface area generated by thermal pretreatment of electrodes reduces its impact on redox flow battery performance, ACS Applied Energy Materials. 4 (2021) 13516–13527.
[56] Y.K. Zeng, X.L. Zhou, L. An, L. Wei, T.S. Zhao, A high-performance flow-field structured iron-chromium redox flow battery, Journal of Power Sources. 324 (2016) 738–744. https://doi.org/10.1016/j.jpowsour.2016.05.138.